(Received 28 July 2024, Accepted 14 October 2024, Scheduled 20 October 2024)

Speed Control of Synchronous Reluctance Motor with Composite Controller Based on Super-Twisting Sliding Mode

Yinhang Ning, Zhihao Huang*, Benqing Lv, Longlong Fu, and Zhaozhuo Li

School of Electrical Engineering, Shanghai Dianji University, Shanghai 201306, China

ABSTRACT: Synchronous reluctance motor (SynRM) has been a hot research topic in recent years. In this paper, a composite speed controller based on the concept of super-twisting sliding mode (STSM) control is designed and innovatively applied to SynRM. For current control, the maximum torque per ampere (MTPA) strategy is used. For torque control, a design method based on an STSM controller is given. In order to solve the chattering phenomenon existing in STSM, a simple structure disturbance observer (DOB) is further introduced as a feed-forward compensation to offset the disturbances. A novel composite sliding mode speed controller is formed based on DOB and STSM. By using Matlab/Simulink, a composite sliding mode speed control system was built. The characteristics of the motor such as current, speed, and torque were researched. Compared to the STSM controller, the speed overshoot of the new controller is reduced by up to 50% (for no-load start). The speed drop is reduced by up to 75% (for sudden load), and the recovery time is shortened by up to 50%. The results show that the designed composite speed control system has better dynamic performance.

1. INTRODUCTION

Synchronous reluctance motor (SynRM) is a new kind of motor scheme without the rare earth, based on the reluctance torque principle, which is one of the current research hotspots. The rotor of this motor is all made of iron cores, which have the advantages of a simple manufacturing process, low cost, and low loss [1]. At present, Asea Brown Boveri (ABB), Tesla, Gree Electric, and other companies have shown a strong interest in SynRM, and have launched related products or prototypes [2]. In 2022, China's Ministry of Industry and Information Technology also listed "developing synchronous reluctance motor" as one of the key tasks, which indicates that the application of SynRM has a broad prospect.

For SynRM control, a model-free predictive current control strategy based on recurrent neural networks is proposed in [3]. This strategy does not require motor parameters, thus avoiding the effects of parameter variations. Ref. [4] applies active disturbance rejection control to SynRM control, and the control strategy is robust to parameter variations. In [5], a nonlinear feedback linearization controller is designed to effectively reduce the impact of parameter changes on performance and improve the dynamic performance of the system. In [6], a minimum loss control strategy considering iron losses is constructed to keep the motor losses at a minimum, which effectively improves the operating efficiency. In order to improve the robustness of speed control, [7] designs a control strategy with adaptive computed q-axis current speed control and d-axis current regulation. In [8], a nonlinear advanced strategy of speed predictive control based on finite control set model predictive control is proposed. The system using this control strategy has a very fast dynamic response without overshooting, but the current and torque fluctuations are large.

Sliding mode control (SMC) is widely used in PMSM control, because of its low influence by parameter variations, high anti-disturbance, and high tracking accuracy [9]. In [10], a suboptimal algorithm second-order SMC controller is proposed, which is robust to changes in motor parameters. Ref. [11] designs a SynRM control strategy combining d-axis current control with adaptive complementary SMC. This strategy improves the speed dynamic response and allows the SynRM to achieve maximum power factor. Ref. [12] proposes an optimal current calculation method and combines it with second-order SMC, which significantly reduces torque pulsations and improves the system performance. However, in practical applications, the SMC controller disturbance upper bound is difficult to determine, and a higher gain value is usually selected to provide sufficient control effort [13], which will aggravate the chattering. Introducing a disturbance observer (DOB) as a feed-forward compensation for the SMC speed controller can estimate and offset the disturbances to solve the chattering [14]. However, at present, this design scheme is mainly applied in PMSMs, and there are few reports of related research in SynRM. In [15] a nonlinear DOB is combined with a non-singular terminal SMC to improve the dynamic performance and robustness of the system. Ref. [16] combines an extended state observer with a disturbance-rejection SMC controller to eliminate the chattering inherent in this controller. However, the observer has at least two or more adjustable parameters, and its structure is relatively complex, which increases the workload of program design and parameter tuning.

Therefore, this paper combines a simple structure DOB with the super twisting sliding mode (STSM) and applies it to the

* Corresponding author: Zhihao Huang (huangzh2097@163.com).

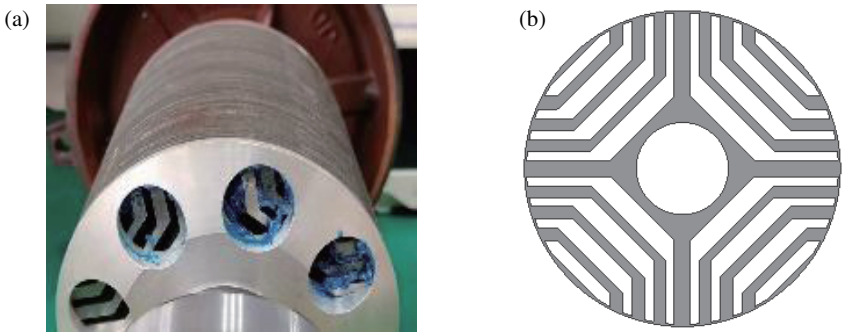

FIGURE 1. SynRM structure. (a) rotor of SynRM. (b) geometrical model of rotor.

SynRM speed control system. For the current control, an MTPA control strategy is used to improve the current utilization. For the torque control, an STSM strategy is used. First, the design method of the STSM controller is given, but it brings chattering due to the high gain value. To solve this problem, a composite controller CSC-DOB-STSM with DOB as feedforward compensation is constructed to eliminate the influence of the disturbance. Finally, the performance of the system is studied by simulation.

The main components of this paper are as follows. In Section 2, the mathematical model of the SynRM system is established. In Section 3, the MTPA control algorithm is derived. The STSM controller, DOB, and CSC-DOB-STSM design process are illustrated. The Liapunov function is constructed to analyze the stability of the controller. In Section 4, the performance of the proposed composite controller is simulated, verified, and compared with the performance of the STSM controller. In Section 5, conclusions are given.

2. SYNRM AND ITS MATHEMATICAL MODEL

The stator of SynRM is the same as the conventional synchronous motor, and the difference is mainly in the rotor, as the rotor of SynRM studied in this paper shown in Fig. 1(a). Fig. 1(b) is the rotor model of SynRM. The rotor is only made of an iron core, and the d-q axis inductances of this motor, L_d and L_q, are not equal. According to the torque generation principle of the motor, it is known that the reluctance torque can be formed when the parameter values of L_d and L_q are unequal. According to parameter identification algorithm, relevant parameters of the motor are obtained and shown in Table 1.

The mathematical model of the SynRM is similar to that of the PMSM, lacking only the rotor flux component. Eq. (1) is the voltage equation of the SynRM in the d-q coordinate system.

$$\begin{cases} u_d = R_s i_d + L_d \dfrac{di_d}{dt} - \omega_e L_q i_q \\ u_q = R_s i_q + L_q \dfrac{di_q}{dt} + \omega_e L_d i_d \end{cases} \tag{1}$$

In Eq. (1), u_d and u_q are stator voltage components on the d-q axis; i_d and i_q are stator current components on the d-q axis; R_s is the stator resistance; and ω_e is the electrical angular velocity.

The electromagnetic torque T_e and mechanical dynamics equations are shown in Eq. (2).

$$\begin{cases} \dfrac{d\omega_m}{dt} = \dfrac{T_e}{J} - \dfrac{T_L}{J} - \dfrac{B}{J}\omega_m \\ T_e = \dfrac{3}{2} p_n \left(Ld - Lq\right) idiq \end{cases} \tag{2}$$

In Eq. (2), ω_m is the mechanical angular velocity, T_L the load torque, B the coefficient of friction, J the rotational inertia, and p_n the number of pole pairs. Based on the electromagnetic torque equation, the field-oriented control strategy with $i_d = 0$ is not applicable to SynRM control.

3. CONTROL STRATEGY OF SYNRM

3.1. MTPA Control

Maximum torque per ampere (MTPA) control is widely used in the control of SynRM, and the basic idea is that, for a given value of output torque T_e, the required minimum stator current is calculated by an algorithm. In principle, the MTPA algorithm can effectively reduce the copper loss of the motor [17]. Eq. (3) gives the basic constraints on the stator current of SynRM, as well as the electromagnetic torque T_e [18].

$$\begin{cases} \min : i_s = \sqrt{i_d^2 + i_q^2} \\ \text{const} : T_e = \dfrac{3}{2} p_n \left(L_d - L_q\right) i_d i_q \end{cases} \tag{3}$$

To realize the above constraints, an auxiliary function as shown in Eq. (4) is constructed, and λ is a Lagrange multiplier.

$$F = \sqrt{i_d^2 + i_q^2} + \lambda \left[T_e - \frac{3}{2} p_n \left(L_d - L_q\right) i_d i_q \right] \tag{4}$$

After the partial derivatives of i_d, i_q, and λ are obtained respectively, the partial derivatives are set to zero, as shown in

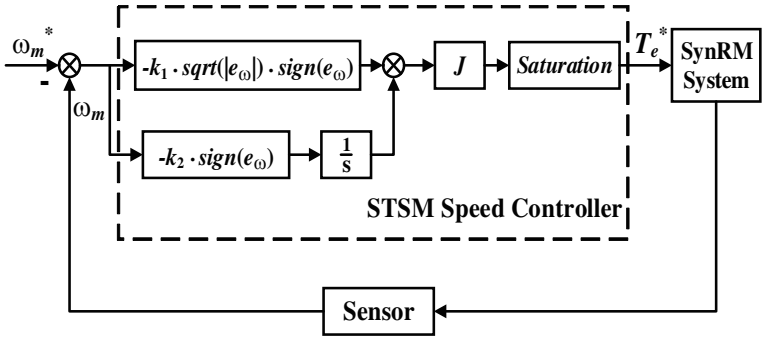

FIGURE 2. STSM speed controller block diagram.

Eq. (5).

$$\begin{cases} \dfrac{\partial F}{\partial i_d} = \dfrac{i_d}{\sqrt{i_d^2 + i_q^2}} - \dfrac{3}{2}\lambda p_n \left(L_d - L_q\right) i_q = 0 \\ \dfrac{\partial F}{\partial i_q} = \dfrac{i_q}{\sqrt{i_d^2 + i_q^2}} - \dfrac{3}{2}\lambda p_n \left(L_d - L_q\right) i_d = 0 \\ \dfrac{\partial F}{\partial \lambda} = T_e - \dfrac{3}{2} p_n \left(L_d - L_q\right) i_d i_q = 0 \end{cases} \tag{5}$$

Solve the first two equations of Eq. (5) to obtain the basic relationship between i_d and i_q, as shown in Eq. (6).

$$i_d = \pm i_q \tag{6}$$

Substituting Eq. (6) into the 3rd equation of Eq. (5), the relationship between T_e and i_q is obtained as shown in Eq. (7).

$$\begin{cases} i_d = i_q,\ T_e > 0 \\ i_q = \sqrt{\dfrac{T_e}{1.5 p_n \left(L_d - L_q\right)}} \end{cases} \text{ and } \begin{cases} i_d = -i_q,\ T_e < 0 \\ i_q = \sqrt{\dfrac{-T_e}{1.5 p_n \left(L_d - L_q\right)}} \end{cases} \tag{7}$$

3.2. Conventional Speed Controller Based on the STSM

For torque control, SMC is used. For the purpose of analysis, define the state variable of the system $s = e_\omega = \omega_m - \omega_m^*$. Eq. (2) is organized into Eq. (8) represented by the state variable s.

$$\begin{cases} \dfrac{ds}{dt} = \dfrac{de_\omega}{dt} = \dfrac{d\omega_m}{dt} - \dfrac{d\omega_m^*}{dt} = -\dfrac{B}{J}\omega_m + \dfrac{1}{J}T_e^* + h\left(t\right) \\ h(t) = -\dfrac{T_L}{J} - \dfrac{1}{J}(T_e^* - T_e) \end{cases} \tag{8}$$

In Eq. (8), ω_m^* is the given mechanical angular velocity, T_e^* the control input, and $h(t)$ the lumped disturbance term. Because T_L, T_e, and T_e^* are all bounded quantities, the lumped disturbance $h(t)$ is bounded. From Eq. (8), it can be seen that the change in the state variable s is jointly influenced by $\frac{T_e^*}{J}$ and $h(t)$.

When designing the speed controller, the STSM control idea is used, and the control relationship is shown in Eq. (9).

$$\begin{cases} \dfrac{ds}{dt} = -k_1 \left|s\right|^{k_3} \text{sign}(s) + u_1 \\ \dfrac{du_1}{dt} = -k_2 \text{sign}(s) \end{cases} \tag{9}$$

In Eq. (9), k_3 is a positive constant $0 < k_3 \leq 0.5$, and k_1 and k_2 are the gain values to be designed.

Different controllers can be obtained by designing the value of k_3. When $k_3 = 0$, it is similar to a constant gain PI controller with a discontinuous function for the input. When $k_3 = 0.5$, it is an STSM controller with the converged finite time. When the state variable $s > 1$, the gain value increases, allowing the system to converge faster to the target state. When $s < 1$, the gain value decreases, which reduces the chattering problem of the system.

For sliding mode control, the desired T_e^* in Eq. (8) can be obtained using Eq. (9). From Eq. (9), it can be seen that a well-designed T_e^* can effectively influence the locus of the state variable s. In conventional speed controllers, only the effect of $\frac{T_e^*}{J}$ is considered. Comparing Eq. (8) and Eq. (9), the speed controller Eq. (10) can be obtained.

$$\begin{cases} T_e^* = J\left[-k_1 \left|e_\omega\right|^{\frac{1}{2}} \text{sign}(e_\omega) + u_1\right] \\ \dfrac{du_1}{dt} = -k_2 \text{sign}(e_\omega) \end{cases} \tag{10}$$

The speed controller built according to Eq. (10) is shown in Fig. 2. In order to prevent the speed error from being too large during startup, which leads to excessive starting current to damage the motor, a limiting module is added to the speed controller.

3.3. Improved Speed Controller (CSC-DOB-STSM)

Conventional speed controllers are designed with only the effect of T_e^* in mind. However, due to the difficulty in defining the upper bound of the disturbance, the gains of k_1 and k_2 are usually designed with large values, which can exacerbate the

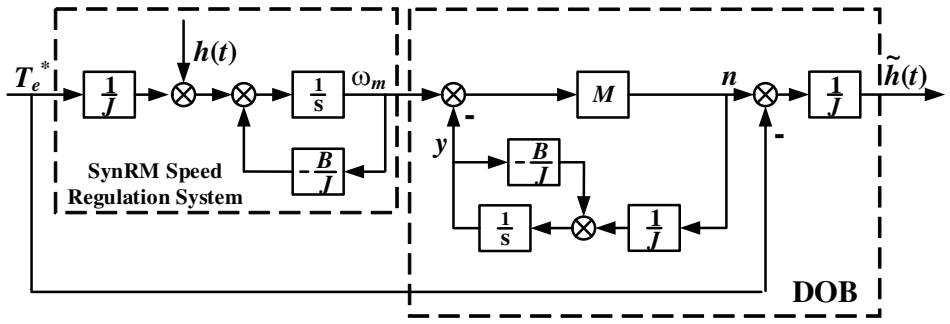

FIGURE 3. DOB block diagram.

chattering. To solve this problem, the effect of the disturbance term $h(t)$ is further considered in Eq. (8). In the speed controller design, a disturbance compensation unit $\tilde{h}(t)$ is added, resulting in a DOB, which can be expressed in Eq. (11)–Eq. (13) [14].

$$\tilde{h}(t) = \frac{1}{J}(n - T_e^*) \tag{11}$$

$$n = M(\omega_m - y) \tag{12}$$

$$\frac{dy}{dt} = -\frac{B}{J}y + \frac{1}{J}n \tag{13}$$

In order to explore the effect of the value of M on the compensation effect of $\tilde{h}(t)$, the following deformation is made from Eq. (11) to Eq. (13).

The derivative of Eq. (12) is substituted into Eq. (13) to obtain Eq. (14).

$$\frac{dn}{dt} = M\left(\frac{d\omega_m}{dt} + \frac{B}{J}y - \frac{1}{J}n\right) \tag{14}$$

Then, Eq. (12) is deformed and substituted into Eq. (14) to obtain Eq. (15).

$$\frac{dn}{dt} = M\left(\frac{d\omega_m}{dt} + \frac{B}{J}\left(\omega_m - \frac{n}{M}\right) - \frac{1}{J}n\right) \tag{15}$$

Rewrite Eq. (15) as Eq. (16).

$$\frac{1}{M} = \frac{\frac{d\omega_m}{dt} + \frac{B}{J}\omega_m}{\frac{dn}{dt} + \frac{B}{J}n} - \frac{\frac{1}{J}n}{\frac{dn}{dt} + \frac{B}{J}n} \tag{16}$$

When M is taken to infinity, Eq. (17) is obtained from Eq. (16).

$$\frac{1}{J}n = \frac{d\omega_m}{dt} + \frac{B}{J}\omega_m \tag{17}$$

Combining Eq. (8) and Eq. (17) yields Eq. (18).

$$\frac{1}{J}n = \frac{1}{J}T_e^* + h(t) \tag{18}$$

The comparison of Eq. (11) and Eq. (18) indicates that at this time $h(t) = \tilde{h}(t)$, which shows that the larger the value of M is, the better the compensation effect is. However, parameter M has a large impact on the dynamic performance of the SynRM control system. The design value should be slowly adjusted from a small initial value until it meets the requirements.

Finally, by combining Eq. (8), Eq. (10), and Eq. (11), this paper proposes the improved speed controller CSC-DOB-STSM as Eq. (19). The corresponding block diagram of the DOB is shown in Fig. 3.

$$\begin{cases} T_{e0}^* = J\left[-k_1 |e_\omega|^{\frac{1}{2}} \operatorname{sign}(e_\omega) + u_1 - \tilde{h}(t)\right] \\ \dfrac{du_1}{dt} = -k_2 \operatorname{sign}(e_\omega) \end{cases} \tag{19}$$

3.4. Stability Analysis of Controller

In order to demonstrate the stability of the speed controller Eq. (19), the Lyapunov constructor is used [19]. Define the Lyapunov function of the speed controller as Eq. (20).

$$V_1 = 2k_2 |e_\omega| + 0.5u_1^2 + 0.5(k_1 |e_\omega|^{0.5} \operatorname{sign}(e_\omega) - u_1)^2 \tag{20}$$

Rewrite Eq. (20) in the form of Eq. (21), and matrix V_1 is positive definite when $k_1 > 0$ and $k_2 > 0$.

$$V_1 = X^T Q X \tag{21}$$

Matrices X and Q are:

$$X = \begin{bmatrix} |e_\omega|^{\frac{1}{2}} \operatorname{sign}(e_\omega) \\ u_1 \end{bmatrix}, \quad Q = \begin{bmatrix} \frac{k_1^2 + 4k_2}{2} & -\frac{k_1}{2} \\ -\frac{k_1}{2} & 1 \end{bmatrix} \tag{22}$$

The derivation of matrix X yields Eq. (23).

$$\begin{cases} \dfrac{dX}{dt} = \dfrac{1}{|e_\omega|^{\frac{1}{2}}} AX + \dfrac{1}{|e_\omega|^{\frac{1}{2}}} E\left(|e_\omega|^{\frac{1}{2}} \dfrac{d\phi}{dt}\right) \\ \dfrac{dX^T}{dt} = \dfrac{1}{|e_\omega|^{\frac{1}{2}}} X^T A^T + \dfrac{1}{|e_\omega|^{\frac{1}{2}}} E^T\left(|e_\omega|^{\frac{1}{2}} \dfrac{d\phi}{dt}\right) \end{cases} \tag{23}$$

Matrices A and E in Eq. (23) are:

$$A = \begin{bmatrix} -\frac{k_1}{2} & \frac{1}{2} \\ -k_2 & 0 \end{bmatrix}, \quad E = \begin{bmatrix} 0 \\ 1 \end{bmatrix} \tag{24}$$

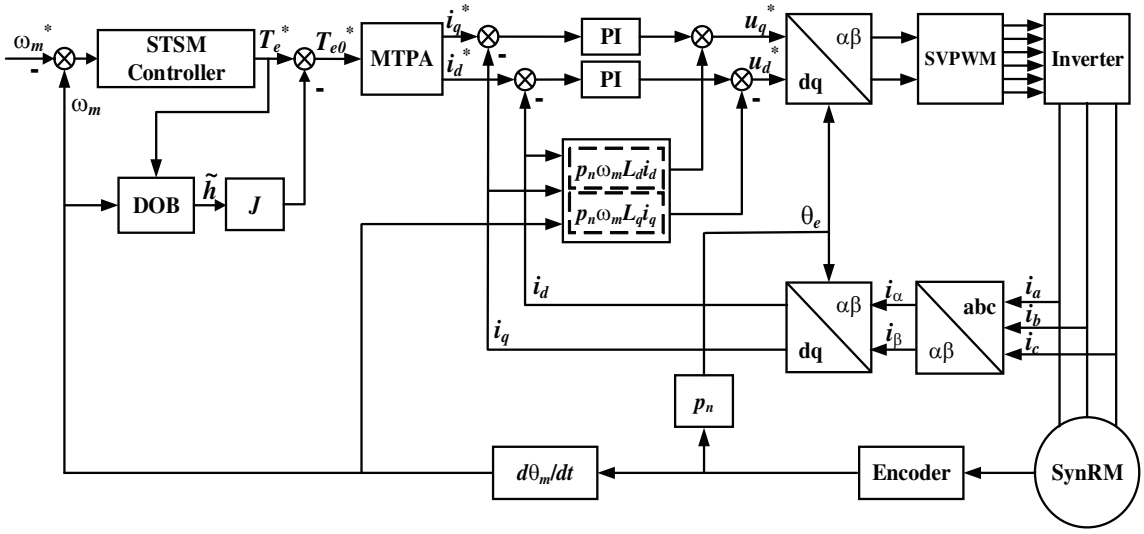

FIGURE 4. Block diagram of SynRM speed control system.

The derivation of Eq. (20) yields Eq. (25), where Φ is the disturbance term.

$$\frac{dV_1}{dt} = \frac{dX^T}{dt}QX + X^TQ\frac{dX}{dt}$$
$$= \frac{1}{|e_\omega|^{\frac{1}{2}}}\left[X^TA^TQX + X^TQAX + \left(|e_\omega|^{\frac{1}{2}}\frac{d\phi}{dt}\right)E^TQX\right.$$
$$\left. + \left(|e_\omega|^{\frac{1}{2}}\frac{d\phi}{dt}\right)X^TQE\right] \tag{25}$$

Since lumped disturbance $h(t)$ is a bounded quantity, there exists $\left|\frac{d\phi}{dt}\right| \le \theta$, with $\theta > 0$ for the disturbance $\phi = h(t) - \tilde{h}(t)$, namely Φ a bounded constant. Since Φ is a bounded constant and $E^TQX = X^TQE$, Eq. (25) can be rewritten as inequality Eq. (26).

$$\frac{dV_1}{dt} \le \frac{1}{|e_\omega|^{\frac{1}{2}}}\left(X^TA^TQX + X^TQAX + \theta^2\left||e_\omega|^{\frac{1}{2}}\right|^2\right.$$
$$\left. + X^TQEE^TQX\right) \tag{26}$$

Rewrite Eq. (26) as Eq. (27).

$$\frac{dV_1}{dt} \le \frac{1}{|e_\omega|^{\frac{1}{2}}}\left(X^TA^TQX + X^TQAX\right.$$
$$\left. + \theta^2X^TB^TBX + X^TQEE^TQX\right) \tag{27}$$

In Eq. (27) $B = [1\,0]$, so $\theta^2X^TB^TBX = \theta^2\|e_\omega|^{0.5}|^2$.

Rewrite Eq. (27) as Eq. (28).

$$\frac{dV_1}{dt} \le -\frac{1}{|e_\omega|^{\frac{1}{2}}}X^TPX \tag{28}$$

In Eq. (28), $P = -[A^TQ + QA + \theta^2B^TB + QEE^TQ]$.

According to matrices A, Q, E, and B, matrix P is obtained as:

$$P = \begin{bmatrix} \frac{k_1^3}{2} - \frac{k_1^2}{4} + k_1k_2 - \theta^2 & -\frac{k_1^2}{2} + \frac{k_1}{2} \\ -\frac{k_1^2}{2} + \frac{k_1}{2} & \frac{k_1}{2} - 1 \end{bmatrix} \tag{29}$$

When $P > 0$, there is $\frac{dV_1}{dt} < 0$ to satisfy the Lyapunov stabilization condition. The speed control system stabilization condition can be given by Eq. (30).

$$\begin{cases} k_1 > 2 \\ k_2 > \dfrac{k_1^3}{4\left(k_1^2 - 2k_1\right)} + \dfrac{\theta^2k_1 - 2\theta^2}{\left(k_1^2 - 2k_1\right)} \end{cases} \tag{30}$$

4. SIMULATION VERIFICATION AND ANALYSIS

To verify the performance of the SynRM speed control scheme based on the composite controller, the corresponding system simulation model is built in Matlab/Simulink. The structural block diagram of the synchronous reluctance motor speed control system is shown in Fig. 4, which mainly includes three functional units such as a CSC-DOB-STSM speed control unit, an MTPA control unit, and the PI regulation of a current unit. In the speed control unit, the desired torque T_e^* is generated using STSM control algorithm according to the speed deviation. The target value of torque after disturbance compensation is T_{e0}^*. In the MTPA unit, for a given T_{e0}^*, the desired current values i_d^* and i_q^* are solved according to Eq. (7). Finally, SynRM speed control is accomplished by the implementation of the PI-based current control unit.

The parameters in the CSC-DOB-STSM are designed with values of $k_1 = 450$, $k_2 = 5000$, and $M = 15$. The design values of k_1 and k_2 satisfy the constraints Eq. (20) for controller stabilization. For the current controller of the d-axis, the PI

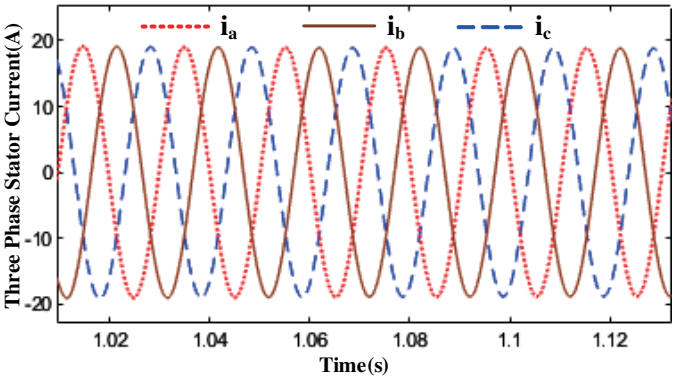

FIGURE 5. Three-phase stator current during stable operation.

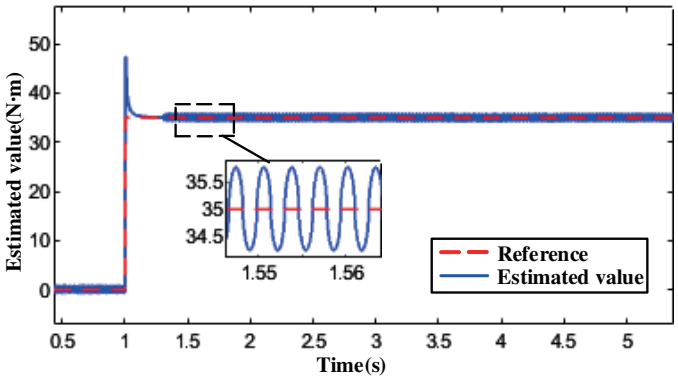

FIGURE 6. Load disturbance observed value.

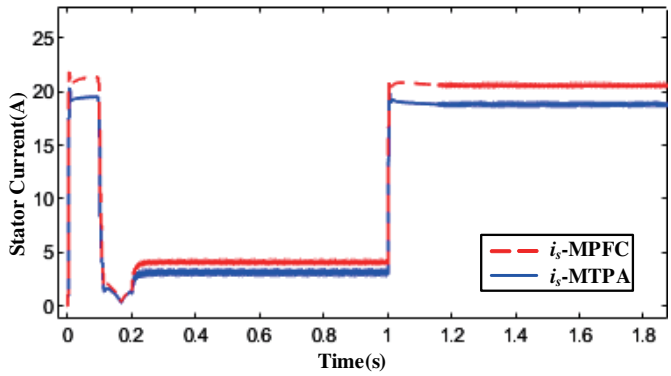

FIGURE 7. Control system stator current.

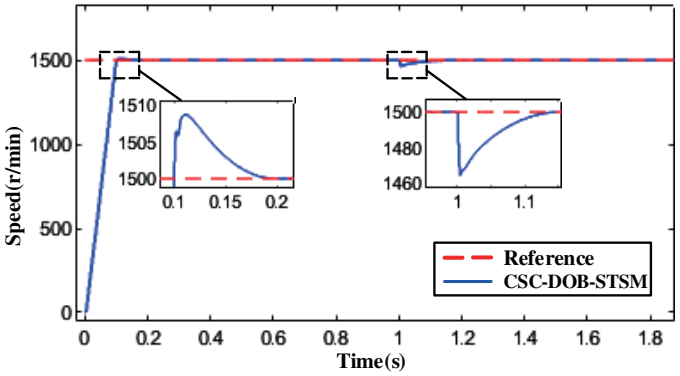

FIGURE 8. Speed control characteristics of the system.

TABLE 1. Parameters of SynRM.

Parameters	Units	Value
Rated current	A	13.5
Rated speed	r/min	1500
Rated torque	N·m	35
Pole pairs/p_n	-	2
Stator resistance/R_s	Ω	2.3
d-axis inductors/ L_d	H	0.0938
q-axis inductors/L_q	H	0.0273
Motorinertia/J	kg·m^2	0.023
Friction coefficient/B	N·m·s	0.0013

parameters are $K_{pd} = 60.59$ and $K_{id} = 529.35$, respectively. For the q-axis, the PI parameters are $K_{pq} = 12.28$, and $K_{iq} = 529.35$, respectively. The parameters of the SynRM used in the simulation, are shown in Table 1.

4.1. Performance Verification of Speed Controller with CSC-DOB-STSM

The three-phase stator currents are shown in Fig. 5 for a given speed value of 1500 r/min and a load value of $T_L = 35$ N·m. The current waveform is basically sinusoidal with an amplitude about 19 A (RMS value about 13.4 A) after the motor speed is stabilized at the rated condition. The observed values of the control system disturbances are shown in Fig. 6. After a step load of 35 N·m is applied at 1 s, it is observed that the DOB can track the load disturbance value better, and there is an error about ± 0.7 N·m after stabilization.

The current variation characteristics of the system are shown in Fig. 7. For the qualitative verification of the current characteristics of MTPA, the current control unit uses MTPA and the maximum power factor control (MPFC) for comparison respectively. In Fig. 7, i_s-MTPA indicates the current amplitude under MTPA control. The i_s-MPFC indicates the current amplitude under MTPC control. Some overshooting of the current occurs during no-load startup for both strategies. But the overshooting for the i_s-MPFC is more serious, about 22 A. The current decreases rapidly after the speed is stabilized. When a step load of 35 N·m is applied at 1 s, i_s-MTPA and i_s-MPFC are both close to the amplitude of the rated current. However, i_s-MTPA is about 15% lower than i_s-MPFC. This is basically consistent with the analysis of MTPA control.

The speed control characteristics of the system are shown in Fig. 8. The speed control system has an overshoot of 9 r/min during no-load startup, and stabilizes at the given speed of 1500 r/min at 0.17 s, with good dynamic performance. 35 N·m load is applied suddenly at 1 s, and the speed falls from 1500 r/min by 38 r/min and recovers to the given speed at 1.11 s, with a short recovery time. The anti-disturbance performance of the system is good.

The electromagnetic torque response curve is shown in Fig. 9. After a sudden load of 35 N·m at 1 s, the torque has a

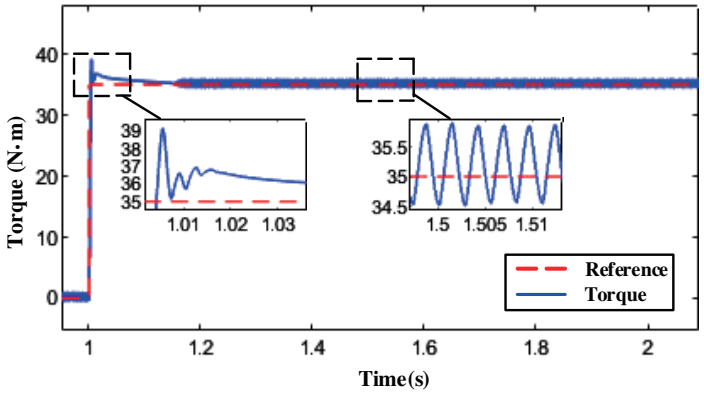

FIGURE 9. Electromagnetic torque response curve.

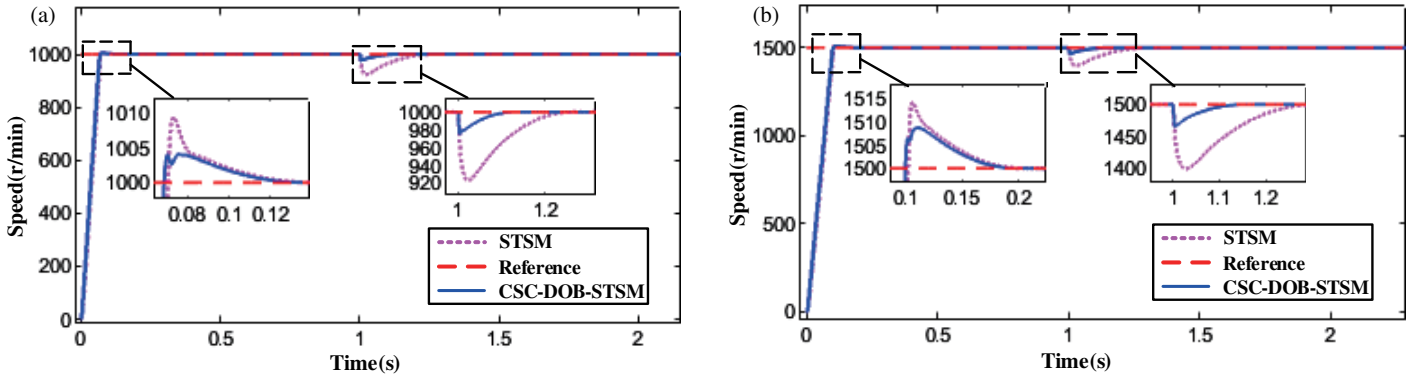

FIGURE 10. Speed response curve at different given speeds. (a) Given speed 1000 r/min, sudden load 30 N·m. (b) Given speed 1500r/min, sudden load 35 N·m.

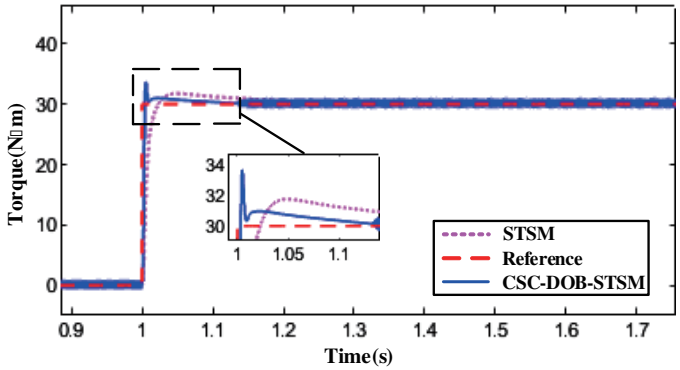

FIGURE 11. Torque response characteristic curve.

maximum overshoot of 4 N·m (about 11.42%) and stabilizes at the given torque within 1.2 s, with a fluctuation of ±1.3 N·m (3.68%) after the torque is stabilized. It can be seen that the speed control system can quickly follow the given torque, and the torque fluctuation after stabilization is small.

4.2. Comparison of STSM and CSC-DOB-STSM Speed Controller Performance

In order to compare with the conventional STSM control, the other units in the simulation system are kept unchanged, and only the speed control unit is adjusted. Fig. 10 gives the speed response curves for a given speed of 1000 r/min and 1500 r/min with CSC-DOB-STSM and STSM control, respectively. A comparison of the anti-disturbance and no-load startup performance of the SynRM speed control system using the two controllers is shown in Table 2 and Table 3. The composite controller reduces the no-load startup speed overshoot by max. 50%, reduces the sudden load speed drop by max. 75%, and reduces the speed recovery time by max. 50%.

The results of the torque response performance comparison are shown in Fig. 11. For the CSC-DOB-STSM-based speed control system, the required time for torque stabilization is sig-

TABLE 2. Comparison of controller no-load startup performance.

Speed (r/min)	Controller	Max speed overshoot (r/min)	Recovery time (s)
1000	STSM	10	0.13
	CSC-DOB-STSM	5	0.13
1500	STSM	14	0.17
	CSC-DOB-STSM	9	0.17

TABLE 3. Comparison of controller anti-disturbance performance.

Speed (r/min)	Sudden Load (N·m)	Controller	Max speed drop (r/min)	Recovery time (s)
1000	30	STSM	80	0.22
		CSC-DOB-STSM	20	0.1
1500	35	STSM	100	0.22
		CSC-DOB-STSM	38	0.11

nificantly less with a sudden load of 30 N·m, but the overshoot is slightly higher than that of the STSM-based system. Therefore, considering the speed and torque response curves, the speed control system based on the CSC-DOB-STSM has better performance in terms of both no-load startup and anti-disturbance performance.

5. CONCLUSION

In this paper, a composite speed controller based on STSM control is researched. The composite controller is innovatively applied to SynRM and verified by simulation.

The main contributions of this paper are as follows.

1. The mathematical model of SynRM is introduced. Based on the control concept of MTPA, the constrained relationship for current control has been deduced.
2. For torque control, an SMC algorithm with the concept of STSM control is researched. The design method of a conventional controller based on this algorithm is also given.
3. For the chattering problem of the conventional controller, a composite controller using DOB as feed-forward compensation is built, and the design principle of DOB is deduced.

The results show that the MTPA control algorithm is realized for current control with a small stator current (obviously less than MPFC). The basic characteristics of the composite and conventional controllers are studied comparatively with the operating conditions such as no-load starting and sudden load change as the background. Simulation results show that the composite controller has better dynamic characteristics. This is reflected in having a smaller amount of overshoot, lower speed drop, and fast recovery capability.

REFERENCES

[1] Shen, J., S. Cai, and S. Yuan, "Analysis and design of Synchronous reluctance machines part I: An overview," *Microwaves*, Vol. 49, No. 10, 72–79, Oct. 2016.

[2] Heidari, H., A. Rassõlkin, A. Kallaste, T. Vaimann, E. Andriushchenko, A. Belahcen, and D. V. Lukichev, "A review of synchronous reluctance motor-drive advancements," *Sustainability*, Vol. 13, No. 2, 729, 2021.

[3] Ahmed, H. M., I. Jlassi, A. J. M. Cardoso, and A. Bentaallah, "Model-free predictive current control of synchronous reluctance motors based on a recurrent neural network," *IEEE Transactions on Industrial Electronics*, Vol. 69, No. 11, 10 984–10 992, Nov. 2022.

[4] Accetta, A., M. Cirrincione, F. D'Ippolito, M. Pucci, and A. Sferlazza, "Robust control of synchronous reluctance motor based on automatic disturbance rejection," *IEEE Open Journal of Industry Applications*, Vol. 5, 209–223, May 2024.

[5] Accetta, A., M. Cirrincione, M. Pucci, and A. Sferlazza, "Feedback linearization based nonlinear control of SynRM drives accounting for self-and cross-saturation," *IEEE Transactions on Industry Applications*, Vol. 58, No. 3, 3637–3651, May-Jun. 2022.

[6] Zhao, Z., Y. Wang, F. Feng, and C. Shen, "Minimum losses control strategy of synchronous reluctance motors considering iron losses," *Electric Machines and Control*, Vol. 27, No. 11, Nov. 2023.

[7] Chen, S.-G., F.-J. Lin, M.-S. Huang, S.-P. Yeh, and T.-S. Sun, "Proximate maximum efficiency control for synchronous reluctance motor via AMRCT and MTPA control," *IEEE/ASME Transactions on Mechatronics*, Vol. 28, No. 3, 1404–1414, Jun. 2023.

[8] Farhan, A., M. Abdelrahem, C. M. Hackl, R. Kennel, A. Shaltout, and A. Saleh, "Advanced strategy of speed predictive control for nonlinear synchronous reluctance motors," *Machines*, Vol. 8, No. 3, 44, Aug. 2020.

[9] Chen, L., H. Zhang, H. Wang, K. Shao, G. Wang, and A. Yazdani, "Continuous adaptive fast terminal sliding mode-based speed regulation control of PMSM drive via improved super-twisting observer," *IEEE Transactions on Industrial Electronics*, Vol. 71, No. 5, 5105–5115, May 2024.

[10] Chiang, H.-K. and W.-B. Lin, "Sub-optimal algorithm second-order sliding mode control for a synchronous reluctance motor speed drive," *Transactions of the Canadian Society for Mechanical Engineering*, Vol. 40, No. 5, 897–908, 2016.

[11] Lin, F.-J., S.-G. Chen, M.-S. Huang, C.-H. Liang, and C.-H. Liao, "Adaptive complementary sliding mode control for synchronous reluctance motor with direct-axis current control," *IEEE Transactions on Industrial Electronics*, Vol. 69, No. 1, 141–150, Jan. 2022.

[12] Aladetola, O. D., M. Ouari, Y. Saadi, T. Mesbahi, M. Boukhnifer, and K. H. Adjallah, "Advanced torque ripple minimization of synchronous reluctance machine for electric vehicle application," *Energies*, Vol. 16, No. 6, 2701, Mar. 2023.

[13] Wang, J., C. Yang, J. Xia, Z.-G. Wu, and H. Shen, "Observer-based sliding mode control for networked fuzzy singularly perturbed systems under weighted try-once-discard protocol," *IEEE Transactions on Fuzzy Systems*, Vol. 30, No. 6, 1889–1899, Jun. 2022.

[14] Ding, S., Q. Hou, and H. Wang, "Disturbance-observer-based second-order sliding mode controller for speed control of PMSM

drives," *IEEE Transactions on Energy Conversion*, Vol. 38, No. 1, 100–110, Mar. 2023.

[15] Ren, L., G. Lin, Y. Zhao, Z. Liao, and F. Peng, "Adaptive nonsingular finite-time terminal sliding mode control for synchronous reluctance motor," *IEEE Access*, Vol. 9, 51 283–51 293, Mar. 2021.

[16] Nasim, U., A. R. Bhatti, M. Farhan, A. Rasool, and A. D. Butt, "Finite-time robust speed control of synchronous reluctance motor using disturbance rejection sliding mode control with advanced reaching law," *Plos One*, Vol. 18, No. 9, e0291042, Sep. 2023.

[17] Xu, X., Y. Wang, and J. Shen, "Direct torque control-space vector modulation control strategy of synchronous reluctance motor based on maximum torque per-ampere," *Transactions of China Electrotechnical Society*, Vol. 35, No. 2, 246–254, Jan. 2020.

[18] Hen, Q., Q. Wang, J. Xu, Z. Zou, and B. Cao, "Comparative research of MTPA control for interior PMSM used in electric vehicles," *Micromotors*, Vol. 50, 32–35, 2017.

[19] Hu, M., H. Ahn, Y. Chung, and K. You, "Speed regulation for PMSM with super-twisting sliding-mode controller via disturbance observer," *Mathematics*, Vol. 11, No. 7, 1618, 2023.